ELSEVIER

Polymer 43 (2002) 6595–6607

polymer

www.elsevier.com/locate/polymer

Free energy of entanglement–condensed systems

Kazuyoshi Iwata*, Mitsuya Tanaka, Naoya Mita, Yoshiyuki Kohno

Department of Applied Physics, Fukui University, Bunkyo 3-9-1, Fukui 910-8507, Japan

Received 31 May 2002; received in revised form 17 June 2002; accepted 21 June 2002

Abstract

Computer simulations of entanglement–condensed systems are performed to study the interaction potential among local-knots (LKs), which are proposed by Iwata and Edwards as basic units of entanglement. By performing hypothetical element-exchange reactions between the system and an external element-bath, chemical potential $\Delta\mu(\chi)$ of chain-elements, measured from its topological equilibrium value, is computed numerically as a function of condensation ratio χ of LKs. $\Delta\mu(\chi)$ is transformed into free energy $\Delta F(\chi)$ of the system, which takes a minimum in the topological equilibrium state ($\chi = 1$) and increases rapidly with increasing χ. It is argued that $\Delta F(\chi)$ comes mainly from the topological repulsive potentials among LKs, because $\Delta F(\chi)$ computed by the simulation is much larger than that predicted by the slip-link model in which the repulsive potential is neglected. To see farther evidences for the repulsive potential among LKs, average length $\bar{L}_a(\chi)$ of each chain a, $a = 1,2,\ldots$, is computed for various χ, and it is found that $\bar{L}_a(\chi)$ changes inversely proportional to χ and roughly proportional to m_a, the number of LKs trapped in chain a; these results are naturally explained by the existence of the repulsive potential among LKs. By tracing motion of LKs along chains using the local Gauss integral introduced in the previous work, it is found that (1) there are many kinds of LKs which have different volumes in the chains according to their complexity but (2) ca. 70 vol% of LKs are the simplest $LK_{2,1}$ which is composed of two stems and has the Gauss integral equal to ± 1. From these results, it is concluded that the validity of LK model is sufficiently proved by the present work. $\Delta\mu(\chi)$ obtained here is applied to crystalline polymers in the next paper (Polymer, 2002;43: (the following paper in this issue)). © 2002 Published by Elsevier Science Ltd.

Keywords: Topological repulsive potential; Local-knot model; Entanglement–condensed system

1. Introduction

The purpose of this work is to study the nature of interaction potentials among local-knots (LKs), which are proposed by Iwata and Edwards [1,2] as elementary units of entanglement. In this model (LK model), entangled polymer chains are represented as shown in Fig. 1, in which LKs are formed among stems (local parts of chains) of length ca. N_e, the average chain length per entanglement. When a pair of stems forms a LK, its Gauss integral takes near integer number $\pm 1, \pm 2, \ldots$, keeping its value until the LK moves to an end of the chains and unfastened. In permanently entangled polymers (such as cross-linked polymers or amorphous domains in stacking lamellar crystals), LKs have essentially an infinite lifetime. It is argued that LKs move like one-dimensional Brownian particles along chains, interacting repulsively with one another and, in a long-time scale, they take part in a corrective motion which is assigned to the reptation motion [3]. LK model is consistent with the reptation/tube model [4–6] in their dynamic behavior but it has many novel features, such as the topological repulsive potential among LKs [1–3], existence of which was assumed from the fact that LKs cannot pass through one another along chains. These behaviors of LKs are confirmed by computer simulations in our previous work [4,5]. To see further evidences for the repulsive interaction among LKs, the previous work is extended here to study the motion of LKs more in detail and to compute the free energy change due to condensation of LKs.

Another purpose of this work is to provide necessary data to the topological theory of crystalline polymers presented in the next paper [6]. In this theory, it is assumed that in the process of crystallization, entanglements existing in the original melt or solution are condensed in amorphous domains and determine the structure of crystals formed. Several people have already discussed this problem. Manderkern [7], for example, argued that crystallinity w_c is determined by the amount of entanglements trapped in the amorphous domains. Strobl [8–10] and Mansfield [11,12]

* Corresponding author.
E-mail address: iwata@polymer.apphy.fukui-u.ac.jp (K. Iwata).

0032-3861/02/$ - see front matter © 2002 Published by Elsevier Science Ltd.
PII: S0032-3861(02)00525-6

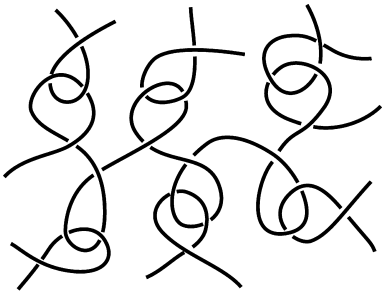

Fig. 1. Local-knot model: entanglement is composed of local-knots which are formed between local chains of length ca. N_e.

considered that the reversible surface melting of lamellae is explained by the thermodynamic equilibrium between the lamellae and entanglement–condensed amorphous domains. In both the phenomena, the basic assumption is that the amount of crystal domains in semi-crystalline polymers is determined by the free energy of entanglement trapped in the amorphous domains. Their arguments are, however, mostly qualitative and insufficient. In studying the role of entanglement in crystalline polymers, the main difficulty is that the usual models of entanglement, such as the reptation/tube model [13–16] or slip-link (SL) model [17], are insufficient to apply to this problem. Although these models are applied successfully to viscoelastic properties of polymers [14], they are insufficient to describe entanglement–condensed systems in which the topological repulsive potentials should play a central role. In this work, chemical potential $\mu(\chi)$ of chain-elements is computed numerically as a function of condensation ratio χ of entanglement and its origin is discussed in terms of the topological repulsive potentials among LKs. $\mu(\chi)$ given here is applied to crystalline polymers in the next paper [6].

2. Chemical potential of chain-elements

The chemical potential of chain-elements introduced here is an unusual but useful concept in studying the role of entanglement in crystalline polymers, which is discussed in the next paper [6]. To show this, we consider a bead-and-spring-model chain of which ends are attached to walls as shown in Fig. 2. The chain is composed of L springs of force constant κ. For simplicity, we first neglect entanglement and the excluded volume among the beads. When the end-to-

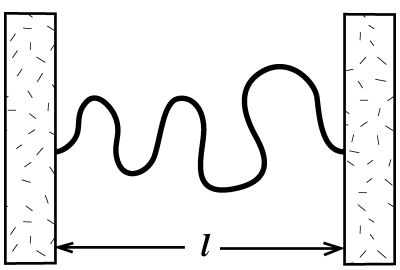

Fig. 2. A linear chain fixed to two walls.

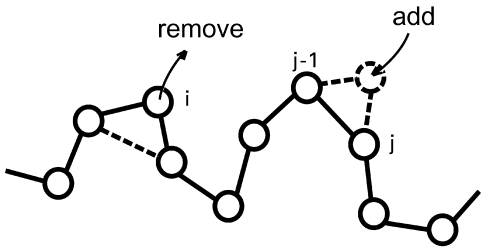

Fig. 3. Imaginary add/remove motions of chain-elements.

end-distance is equal to l, the free energy of the chain is given by

$$\beta F(L,l) = \text{constant} + \frac{3}{2}\ln L + \frac{3l^2}{2La^2}, \tag{1}$$

where $a^2 = 3k_BT/\kappa$ is the mean-square length of the springs and β has the usual meaning, $\beta = 1/k_BT$. This is a simplified model of an amorphous domain in stacking lamellar crystals; the walls represent surfaces of lamellae and the chain, a tie molecule in the amorphous domain. Chemical potential $\mu(L,l)$ of chain-elements is given under this condition by

$$\begin{aligned}\beta\mu(L,l) &= \beta[F(L,l) - F(L-1,l)] \\ &= (3/2L)(1 - l^2/La^2)\end{aligned} \tag{2}$$

for $L \gg 1$.

Now, we show that $\mu(L,l)$ is computed by a Monte-Carlo simulation of an imaginary element-exchange reaction between the chain and an external element-bath as follows. When bead i is removed form the chain as shown in Fig. 3, change of the energy due to the reaction is equal to $\Delta E = -\kappa\mathbf{b}\cdot\mathbf{b}'$, where $\mathbf{b}$ and $\mathbf{b}'$ are bond vectors connecting element i. The bond-formation energy associated with this reaction is assumed to be zero. Addition or removal of elements are done with the following probabilities

$$\begin{aligned} p_a &= p^0 && \text{for addition} \\ p_r &= p^0\exp(\beta\,\Delta E) && \text{for removal}\end{aligned} \tag{3}$$

where p^0 is a positive constant, which makes p_a and p_r always less than unity. By Eq. (3), the detailed Boltzman's balance holds always in the reaction. When elements are exchanged between the chain and an external element-bath of chemical potential μ, extra work μ needs to take an element from the bath; in this case, addition should be done with probability $p'_a = p_a\exp(-\beta\mu)$. When the equilibrium between the chain and the element-bath is established, the number of additions and removals of the chain elements should be the same or $\langle p'_a\rangle$ should be equal to $\langle p'_r\rangle$, where $\langle\ \rangle$ is an average over the equilibrium distribution of the chain with l fixed. Thus we find

$$\beta\mu = \ln[\langle p_r\rangle/\langle p_a\rangle], \tag{4}$$

$$\beta\mu = -\ln\langle\exp(\beta\Delta E)\rangle. \tag{5}$$

Inserting $\Delta E = -\kappa \mathbf{b}\cdot\mathbf{b}'$ into Eq. (5) and taking the average over the equilibrium distribution of the chain with l fixed, Eq. (5) gives Eq. (2) exactly. Thus, $\mu(L, l)$ can be computed by performing the imaginary element-exchange reaction and using Eq. (4).

Now let us show that Eqs. (4) and (5) hold generally in any system composed of identical repeating units. Particularly, we consider a catena network (permanently entangled cyclic polymer chains), in which entanglement states among the chains are conserved and excluded volume potentials act among the chain-elements. Generally, let $\mathscr{R}$ be a set of given restrictive conditions such as the fixed end-to-end-distance l or given topological states of the system. $\mathscr{R}$ includes macroscopic conditions such as volume V, temperature T and pressure P of the system. Let $E_n\{\mathbf{n}\}$ and $E_{n-1}\{\mathbf{n}-1\}$ be energies of systems composed of n and $n-1$ elements, respectively, where $\{\mathbf{n}\}$ and $\{\mathbf{n}-1\}$ represent set of coordinates of the all elements in the system. The chemical potential of the system is given by

$$\mu(n, \mathscr{R}) = F(n, \mathscr{R}) - F(n-1, \mathscr{R}), \tag{6}$$

where $F(n, \mathscr{R})$ and $F(n-1, \mathscr{R})$ are the free energies of the system defined by

$$\beta F(n, \mathscr{R}) = -\ln \int_{\mathscr{R}} \exp(-\beta E_n\{\mathbf{n}\}) \mathrm{d}\{\mathbf{n}\}, \text{ etc.} \tag{7}$$

The integration should be performed over the all space under restriction $\mathscr{R}$. For simplicity, the momentum space is neglected. Now, elements are exchanged between an external bath of chemical potential μ with the add/remove probability given by Eq. (3) in which ΔE is given by

$$\Delta E\{\mathbf{n}\} = E_n\{\mathbf{n}\} - E_{n-1}\{\mathbf{n}-1\}. \tag{8}$$

By the same reason as discussed above, μ is given by Eqs. (4) and (5), where average $\langle\ \rangle$ should be performed over equilibrium distribution

$$P_e\{\mathbf{n}; \mathscr{R}\} = \exp(-\beta E_n\{\mathbf{n}\}) / \int_{\mathscr{R}} \exp(-\beta E_n\{\mathbf{n}\}) \mathrm{d}\{\mathbf{n}\}. \tag{9}$$

We thus find

$$\begin{aligned}\langle \exp(\beta \Delta E) \rangle &= V^{-1} \int_{\mathscr{R}} \exp(\beta \Delta E_n\{\mathbf{n}\}) P_e\{\mathbf{n}; \mathscr{R}\} \mathrm{d}\{\mathbf{n}\} \\ &= \int_{\mathscr{R}} \exp(-\beta E_{n-1}\{\mathbf{n}-1\}) \mathrm{d}\{\mathbf{n}-1\} / \\ &\quad \int_{\mathscr{R}} \exp(-\beta E_n\{\mathbf{n}\}) \mathrm{d}\{\mathbf{n}\},\end{aligned} \tag{10}$$

where V is the volume of the system. Insertion of this equation into rhs of Eq. (5) gives Eq. (6). Thus, chemical potential $\mu(n, \mathscr{R})$ of any system can be computed using Eq. (4) by performing imaginary element-exchange reactions with add/remove probabilities satisfying given restrictive condition $\mathscr{R}$ and the detailed Boltzman's balance.

By the premise of the imaginary element-exchange reaction considered here, the bond-formation energy is not included in $\mu(n, \mathscr{R})$. It is therefore equal to the work necessary for pulling a chain by one element out from the system or it represents a 'tensile force' acting along the chain under the restrictive condition $\mathscr{R}$. This tensile force is different from that assumed in the tube model [14–16].

3. Model of simulations

3.1. Bond-fluctuation (BF) model

We use here BF model which is often used in the simulations of entangled polymers [18–20]. In this model, polymer chains are restricted on a simple-cubic lattice and chain-elements are represented by unit cubes (consisting of eight lattice points) connected by bonds of length b, $2 \le b \le \sqrt{10}$. There are in total 108 bonds satisfying these conditions and they are classified into six basic types: (2,0,0), (2,1,0), (2,1,1), (2,2,1), (3,0,0) and (3,1,0). The mutual avoiding condition (excluded volume condition) among elements is assumed. Elementary processes of the Brownian motion are random moves of elements by unit length in $\pm x$, $\pm y$ or $\pm z$ direction; this motion is hereafter called 'local motions'. We have later found that the original model proposed by Paul et al. [18] contains vital defects called X-traps, which gives errors in the long-time behavior of the system, and proposed a modified BF model which is free from X-traps [19]. Details of the model and X-traps should be referred to Ref. [19]. In this work, the corrected BF model is used.

3.2. Element-exchange motions (add/remove motion)

Beside with the local motions considered in the original BF model, we introduce here newly add/remove motions of elements shown in Fig. 3. When an element chosen randomly, say i, is removed, new bond $\mathbf{b}(i-1, i+1)$ is formed between element $i-1$ and $i+1$; new bond $\mathbf{b}(i-1, i+1)$ should satisfy the restrictive conditions for bonds (i.e. it should be one of the 108 bonds permitted for BF model), otherwise the removal motion is rejected. In addition motion, a bond, say j, is chosen randomly and new element j' is inserted between element $j-1$ and j; as j' is added, two new bond $\mathbf{b}(j-1, j')$ and $\mathbf{b}(j', j)$ are formed, which should satisfy the restrictive conditions for bonds; in the addition motions, there are many possible positions for addition to each bond, to one of which chosen randomly a new element is added, if the position is not occupied by other elements; unless all of these conditions satisfied, the motion is rejected. These add/remove motions are defined for intermediate elements of the chains. For linear chains, terminal elements are also added and removed but their add/remove motions should be modified slightly; however, its precise description is omitted here, since the modifications are straightforward and the most calculations are done for cyclic chains. In the add/remove motions, further

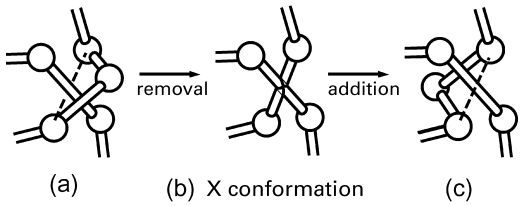

Fig. 4. X-mechanism for passing through chains (two-steps process).

restrictions must be introduced to inhibit crossing among chains. There are the following two mechanisms for crossing chains by the add/remove motions.

X-mechanism: Pairs of bonds of (2,2,1) and (3,1,0)-type form what we call X-traps as shown in Fig. 4b [19]. There are in total 48 X-traps formed by (2,2,1)-type pairs, say (2,2,1) and (−2,2,1), and 24 X-traps formed by (3,1,0)-type pairs, say (3,1,0) and (1, −3,0). The local motions never form these X-traps. They are formed when new bonds are formed in the add/remove motions. Suppose that element i of chain a, which is initially in the conformation shown in Fig. 4a, is removed to form a X-trap between new bond $\mathbf{b}(i-1, i+1)$ and bond j of chain b (Fig. 4b), and then a new element is added to $\mathbf{b}(i-1, i+1)$ as shown in Fig. 4c, then, chain a passes through chain b. These are two-step passing processes named 'X-mechanism'.

Δ-mechanism: In BF model, what is named Δ-conformations appear, in which three bonds of (2,2,1) and (3,1,0)-type form a triangle and another bond of (2,2,1)-type passes through it as shown in Fig. 5; for example, bond (2,2,1), (−1, −2,2) and (−1,0, −3) form triangle $A_1A_2A_3$ and bond (2, −2, −1) passes through it. There are in total 48 such conformations. Suppose that bond (2,2,1) and (−1, −2,2) are a part of chain a and bond (2, −2, −1), a part of chain b; when element A_2 is removed and new bond (−1,0, −3) is formed, then, chain a passes through chain b. This is one step passing process named 'Δ-mechanism'.

By inhibiting the X- and Δ-mechanisms in the add/remove motions, chains never pass through one another. This is confirmed by calculating Gauss integrals among cyclic chains. In this work, the following four types of the add/remove motions are considered: (a) intra-chain element-exchange motion (sliding motion), (b) inter-chain element-exchange motion, (c) element-exchange reactions between the system and an external bath and (d) macroscopic deformation of the system.

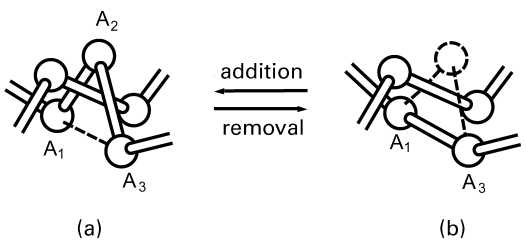

Fig. 5. Δ-mechanism of passing through chains (one-step process).

(a) *Element-exchange motion within each chain* (*sliding motion*): An element of a chain, say i, is removed and added to a bond, say j, of the same chain. This motion looks like a sliding motion of the part of the chain between i and j by one bond along the contour of the chain. In the sliding motion, chain lengths are conserved. The sliding motions equilibrate the system rapidly, so that they are useful to get an equilibrium ensemble with chain-lengths fixed.

(b) *Element-exchange motion among different chains in the system*: Exchange is done among the all chains in the system. In this motion, chain lengths are not conserved but the total number of elements is fixed.

(c) *Element-exchange motion between the system and an external element-bath*: Elements are exchanged between the system and an external bath of chemical potential of μ. A same number of trials of addition and removal are done per unit time. Factor $\exp(-\beta\mu)$ is multiplied to addition probability p_a when $\mu \geq 0$, and factor $\exp(\beta\mu)$, to removal probability p_r when $\mu < 0$. In this motion, chain lengths and the total number of elements of the system are fluctuating around their average values. This motion is used to compute chemical potential of elements using Eq. (4).

(d) *Macroscopic deformation of the system*: To deform the macroscopic shape of the system in BF model, planes are inserted or removed from the simple-cubic lattice on which the chains are restricted. Insertion or removal of plane S perpendicular to, say, the x axis of the lattice is done as follows. First, the all bonds passing through or locating on S are moved so that they are all vertical to S. Before removing plane S, the all bond vectors passing through it must be either of (±3,0,0), (±3, ±1,0) or (±3,0, ±1), which change into (±2,0,0), (±2, ±1,0) or (±2,0, ±1), respectively, after removal of plane S. Before insertion of plane S, the all bonds passing through it are moved so that they are either of (±2,0,0), (±2, ±1,0) or (±2,0, ±1), which change into (±3,0,0), (±3, ±1,0) or (±3,0, ±1), respectively, after insertion of S. These processes are done by the local motions so that the topological state of the system is conserved strictly. Removals and insertions of planes are repeated until the system deforms to a desired form. Just after finishing the deformation, the system is far from its equilibrium state; equilibration of the system is done by the element-exchange motions among the chains or between the system and an external element-bath according to the problem considered.

The add/remove motions introduced here satisfy the detailed Boltzman's balance. In fact, energy change ΔE due to an add/remove motion becomes infinite (or $\exp(-\beta\Delta E) = 0$), when newly formed bonds violate the required condition for bonds or an inserted element overlaps with other elements, thus the motion does not occur. When the motion satisfies the required conditions, ΔE is equal to zero (or $\exp(-\beta\Delta E) = 1$), since the all permitted conformations have the same energy in BF model; thus the motion

Table 1
Bond type distribution in the local and add/remove motion (in the topological equilibrium state)

Bond type	Local motion	Add/remove motion
(2,0,0)	0.0911	0.0913
(2,1,0)	0.2727	0.2733
(2,1,1)	0.2237	0.2243
(2,2,1)	0.2176	0.2167
(3,0,0)	0.0376	0.0375
(3,1,0)	0.1572	0.1568

is always permitted. This is consistent with the definition of add/remove probabilities, p_a and p_r, given by Eq. (3). Since both the local and add/remove motion satisfy the detailed Boltzman's balance, they should give the same equilibrium states. To confirm this, two kinds of simulations, one by the local motions alone and the other by the add/remove motions (the intra-chain element-exchange motions) alone, are performed for linear chains and it is found that equilibrium quantities, such as radius of gyration $\langle R_g^2 \rangle$, mean-square end-to-end distance $\langle L^2 \rangle$ and the bond type distribution, agree well in the two simulations within the statistical error. As an example, the bond type distributions found in the two simulations are shown in Table 1. Thus, both of the local and add/remove motions give the same equilibrium states. The two motions, however, have mutually complementary characters. The local motions change local conformations rapidly while the add/remove motions change long-range conformations of the chains efficiently. To compensate the defects of the two motions, they are mixed with an equal ratio in the simulations; i.e. the chains are moved by the local motions for 1 ut (1 unit time = 1 Monte-Carlo cycle) and then by the add/remove motions for 1 ut. Hereafter, 1 ut means 1 ut of the local motions plus 1 ut of the add/remove motions.

4. Calculation of the chemical potential and free energy in entanglement–condensed systems

4.1. Topological equilibrium state

As a standard state of entanglement, we consider the 'topological equilibrium state', which is defined as the equilibrium state of equivalent phantom chains [21]. Difference between real and phantom chains is that the former cannot pass through one another, while the latter can. For linear chains, there is no difference between the equilibrium states of real and phantom chains, because entanglement states (or LKs) are changing in the both systems. On the other hand, in the catena networks and network polymers, entanglement stats are kept in real chains while they are not in phantom chains. Since entanglement states of these systems are determined when they are formed, we must consider how they are prepared. Ideally, network polymers are in the topological equilibrium state just after cured; i.e. if cross-linking reaction proceeds so slowly that the equilibrium between trapped and free chains is sustained during the reaction, the trapped entanglements must be in the topological equilibrium state [21]. Actually, the reaction proceeds with a considerable rate so that the trapped entanglements will be more or less deviate from their topological equilibrium state; we should therefore ask how far their just-cured states deviate from their topological equilibrium. In stacking lamellar crystals discussed in the next paper [6], we need to know the free energy difference between the equilibrium melt and entanglement–condensed amorphous domains. In these problems, the topological equilibrium state is the only possible standard state for trapped entanglements. In the present works, initial conformations of the system are chosen from the equilibrium ensemble of phantom cyclic chains so that they have typical conformation in the topological equilibrium state.

4.2. Simulation systems

The system is composed of 32 cyclic chains (BF model) restricted on a simple-cubic-lattice. The periodical boundary condition is assumed and the volume fraction of the chains is fixed to $\phi = 0.5$ throughout this work. Initially, the chains have equal length 512 and the volume of the system is equal to $64 \times 64 \times 64$. The chains are initially packed randomly neglecting the excluded volume condition and then equilibrated by the local and add/remove motion, permitting partial overlap among the elements. In the equilibration process, overlapping probability $P_{overlap}$ is changed very slowly to zero and, in the sampling process of initial conformations, $P_{overlap}$ is changed periodically between zero and a small positive number, 0.05. In these processes, the chains pass through one another so that the system approaches to the topological equilibrium state. The initial equilibration process is continued until R_g and the distribution of bond length reaches their expected equilibrium values. Three independent initial conformations are chosen from the equilibrium ensemble and X- and Δ-conformations are removed from them by the method described in the previous paper [19]. Samples made from these initial conformations are designated as S_1, S_2 and S_3.

4.3. Calculation of chemical potentials in closed systems

The system is then deformed isotropically or uniaxially by the method described above. Details of deformation are shown in Table 2. Uniaxial deformation is a model of the lamellar thickening process in stacking lamellar crystals, discussed in the next paper [6]. Isotropic deformation is considered for reference as the simplest case. After

Table 2
Results for isotropic and uniaxial deformation

Cell size	χ	p_a	p_r	$\beta\Delta\mu$
Isotropic deformation				
$80\times80\times80$	0.512	0.1091	0.2996	0.0179
$64\times64\times64$	1	0.1092	0.2944	0
$52\times52\times52$	1.864	0.1092	0.2807	−0.0472
$44\times44\times44$	3.08	0.1091	0.2517	−0.1556
$40\times40\times40$	4.10	0.1087	0.2206	−0.2883
$36\times36\times36$	5.62	0.1083	0.1675	−0.5554
Uniaxial deformation				
$64\times64\times64$	1	0.1092	0.2945	0
$32\times64\times64$	2	0.1092	0.2765	−0.0636
$20\times64\times64$	3.2	0.1090	0.2376	−0.2135
$16\times64\times64$	4	0.1086	0.2008	−0.3778
$13\times64\times64$	4.92	0.1080	0.1510	−0.6564

Average over the forward and reverse deformation of sample S_1 and the forward deformation of sample S_2.

deformation, the system is equilibrated for a sufficiently long time (1–10 Mut) by the local motion + add/remove motions. Since elements are added to and removed from the chains randomly, chain-lengths fluctuate but the volume fraction of elements is kept always at $\phi = 0.5$. In these processes, the chains cannot pass through one another so that entanglements (LKs) are conserved. Condensation ratio χ of LKs is given by $\chi = V_0/V$, where V_0 is the initial volume of the system. To confirm for the equilibrium states to be established well in each deformation step, the system is deformed step-by-step to the maximum deformation state (forward deformation), in each step, the system being well equilibrated and then, it is returned to the initial state in the similar manner (return deformation). The simulation is done for initial conformation S_1 and S_2. To compute chemical potential $\mu(\chi)$ using Eq. (4), addition and removal probability, $\langle p_a\rangle = \langle N_a\rangle/N$ and $\langle p_r\rangle = \langle N_r\rangle/N$, are computed, where N is the total number of the elements, N_r the total number of successful removal, and N_a is the total number of successful additions of elements per unit time; $\langle\ \rangle$ represents average over the samples. Chemical potential $\mu(\chi)$ is thus computed with the use of Eq. (4) as functions of χ for uniaxial and isotropic deformation. In the most problems, it is sufficient to know the difference of $\mu(\chi)$ from its topological equilibrium value, $\Delta\mu(\chi) \equiv \mu(\chi) - \mu(1)$. $\Delta\mu(\chi)$ computed for initial conformation S_1 and S_2 in the forward and reverse deformation are separately shown in Fig. 6. As seen from the figure, the deviations between the forward and reverse deformation are quit small; this indicates that the system is well equilibrated in each deformation step. The deviations between S_1 and S_2 are also small and may be neglected. The average of $\langle p_a\rangle$, $\langle p_r\rangle$ and $\beta\Delta\mu$ for the forward and reverse deformation of sample S_1 and the forward deformation of S_2 are given in Table 2.

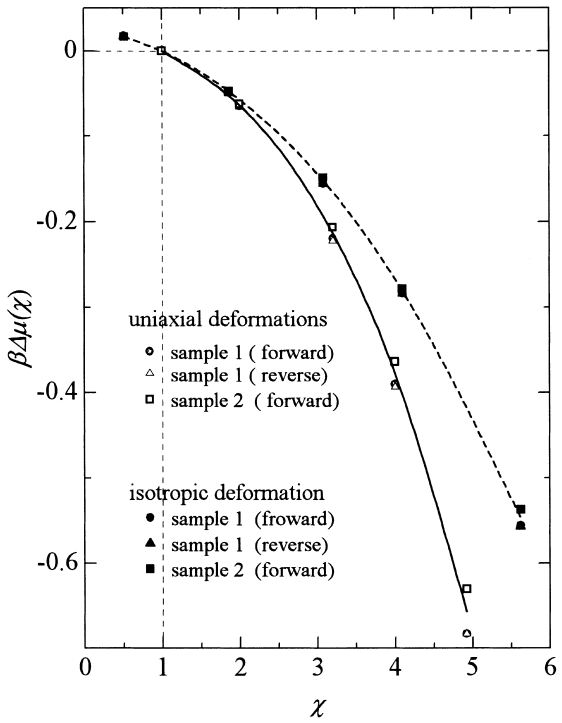

Fig. 6. Chemical potential $\beta\Delta\mu(\chi)$ of chain-elements plotted against condensation ratio χ of LKs.

$\beta\Delta\mu(\chi)$ obtained here is fitted numerically by

$$\beta\Delta\mu(\chi) = \begin{cases} 0.03963 - 0.0369\chi + 0.00199\chi^2 - 0.00472\chi^3 & \text{(uniaxial)}, \\ 0.02876 - 0.0160\chi - 0.0122\chi^2 - 0.00056\chi^3 & \text{(isotropic)} \end{cases} \quad (11)$$

$\beta\Delta\mu(\chi)$ computed by Eq. (11) is shown by straight line (uniaxial deformation) and broken line (isotropic deformation) in Fig. 6.

4.4. Open systems

Strictly speaking, $\Delta\mu(\chi)$ determined above is not the exact chemical potential, because it is computed in the closed systems. Thermodynamically, it should be determined in open systems in which elements are exchanged with an external bath. In principle, simulation of the open system is done as follows. After deforming the system to V, it is equilibrated by element-exchange reaction with an external bath of chemical potential μ; the exact chemical potential is given by such μ that makes the average volume fraction of the elements, $\bar{\phi}$, equal to the prescribed value, $\phi = 0.5$. This method, however, takes much computational time and is difficult to perform by the computers used in this work. The difference between the open and

Table 3
$\bar{\phi}$ and $\sqrt{\langle(\phi/\bar{\phi}-1)^2\rangle}$ for isotropic deformations in open systems

χ	$\beta\mu$	$\bar{\phi}$	$\sqrt{\langle(\phi/\bar{\phi}-1)^2\rangle}$
5.62	0.4363	0.50052	0.00386
4.10	0.7084	0.50070	0.00356
3.08	0.8361	0.50050	0.00318
1.86	0.9445	0.50048	0.00256
1.00	0.9917	0.50036	0.00191
0.51	1.0096	0.50054	0.00137

Average over the forward and reverse deformation in the closed systems of sample S_1.

closed system is that, in the former, ϕ is fluctuating around 0.5, while in the latter, it is exactly fixed to 0.5. Since the fluctuation of ϕ is of the order of $1/\sqrt{N}$, N, the total number of elements in the system, the difference must be much smaller than the statistical errors in the present simulations. To see the difference between the closed and open systems, the closed system for which $\mu(\chi)$ has been already determined as shown in Table 2 is further equilibrated by element-exchange reaction with an external bath of the same chemical potential, $\mu(\chi)$. By this element-exchange reaction, ϕ fluctuates but its time-average $\bar{\phi}$ was almost equal to the prescribed value, 0.5, and the width of concentration-fluctuation $\sqrt{\langle(\phi/\bar{\phi}-1)^2\rangle}$ was very small as shown in Table 3. This result suggests that $\mu(\chi)$ computed in the closed system (Table 2) must be very close to its exact values in the open system.

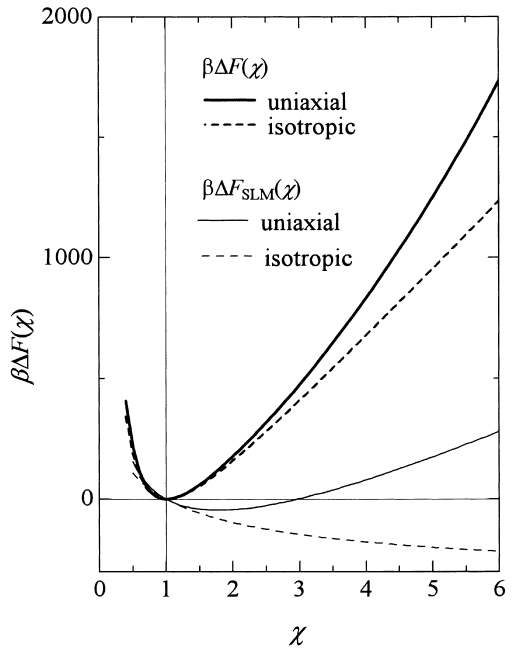

Fig. 7. Total free energy of the system $\beta\Delta F(\chi)$ plotted against condensation χ of LKs. Thin lines represent $\beta\Delta F_{\mathrm{SLM}}(\chi)$ computed by the SL model.

4.5. Total free energy change of the system $\Delta F(\chi)$

It is given by

$$\beta\Delta F(\chi) = \int_{N_0}^{N} \Delta\mu(N_0/N')\mathrm{d}N'$$
$$= \begin{cases} 323\chi^{-1} - 464 + 180\ln\chi + 137\chi + 3.15\chi^2 & \text{(isotropic)}, \\ 445\chi^{-1} - 462 + 414\ln\chi - 22.4\chi + 39.6\chi^2 & \text{(uniaxial)}, \end{cases} \quad (12)$$

where N_0 is the total number of elements in the initial conformation ($N_0 = 16,384$). Pictures of $\beta\Delta F(\chi)$ are shown in Fig. 7 (bold straight and dotted lines).

5. Comparison with the slip-link model

To study the surface melting phenomena in stacking lamellar crystals, Riger and Mansfield (RM) [11,12] computed $\Delta F(\chi)$ using the SL model [17]. In this model, entanglements are represented by small links (slip-links), which move smoothly but cannot pass one another along the chains (Fig. 8). SL model may look like LK model, but there is an important difference between them. In LK model, strong repulsive forces act among LKs but they are absent in SL model. If $\Delta F(\chi)$ comes mainly from the topological repulsive potentials among LKs, as we assume, there must be a large difference between $\Delta F(\chi)$ computed in this simulation and that predicted by SL model. This is therefore a good test for the topological repulsive potentials among LKs.

Following RM [11,12] we assume that the system is composed of $\nu_s = N_0/N_e$ strands of length L_i ($i = 1, 2, \ldots, \nu_s$) and its free energy is given by

$$\beta F_{\mathrm{SLM}}(\Lambda) = \frac{3}{2}\sum_{i=1}^{\nu_s}(\ln L_i + \mathbf{l}_i^2/L_i a^2), \quad (13)$$

where $\mathbf{l}_i = (l_{ix}, l_{iy}, l_{iz})$ is the end-to-end vector of strand i and $\Lambda = (\lambda_x, \lambda_y, \lambda_z)$ is the extension ratio of the system. Eq. (13) is a natural extension of Eq. (1). In the present system, ν_s is

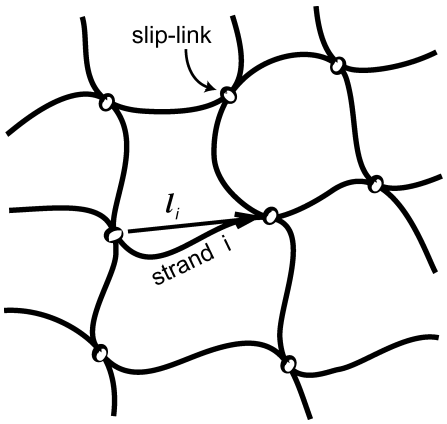

Fig. 8. SL model.

estimated to be 148 using $N_e = 89$ determined previously for BF model at $\phi = 0.5$ [19]. When the system is in equilibrium with a linear chain melt, the average of $\mathbf{l}_i^2/L_i a^2$ over the strands is equal to $\langle(\mathbf{l}_i^0)^2/L_i^0 a^2\rangle = 1$, where L_i^0 and $\mathbf{l}_i^0$ are L_i and $\mathbf{l}_i$ in the equilibrium melt. By deformation to $\Lambda = (\lambda_x, \lambda_y, \lambda_z)$ with $\phi = 0.5$ fixed, slip-links are condensed to concentration ratio $\chi(= N_0/N = 1/\lambda_x\lambda_y\lambda_z)$. Following RM [11,12], it is assumed that L_i changes linearly proportional to the total number of elements, N, and $l_{i\xi}$ ($\xi = x, y, z$) changes affinely as

$$L_i = L_i^0/\chi \quad \text{and} \quad l_{i\xi} = l_{i\xi}^0\lambda_\xi. \tag{14}$$

For isotropic deformation $\Lambda = (\chi^{-1/3}, \chi^{-1/3}, \chi^{-1/3})$ and uniaxial deformation $\Lambda = (\chi^{-1}, 1, 1)$, Eq. (13) gives the free energy relative to its equilibrium melt value

$$\beta\Delta F_{\mathrm{SLM}}(\chi) = \frac{3\nu_s}{2}\begin{cases} \chi^{1/3} - 1 - \ln\chi & \text{(isotropic)}, \\ 2\chi/3 + 1/3\chi - 1 - \ln\chi & \text{(uniaxial)}. \end{cases} \tag{15}$$

Uniaxial case in Eq. (15) has been derived by RM [11,12]. $\Delta F(\chi)$ and $\Delta F_{\mathrm{SLM}}(\chi)$ are compared in Fig. 7. Generally speaking, $\Delta F_{\mathrm{SLM}}(\chi)$ is much smaller than $\Delta F(\chi)$. Particularly for the isotropic condensation ($\chi > 1$), $\Delta F(\chi)$ increases rapidly while $\Delta F_{\mathrm{SLM}}(\chi)$ decreases with increasing χ; thus, SL model cannot describe the change due to the isotropic condensation. In the uniaxial condensation, on the other hand, $\Delta F_{\mathrm{SLM}}(\chi)$ changes considerably and increases with increasing χ above $\chi > 1.6$; thus $\Delta F_{\mathrm{SLM}}(\chi)$ should give a part of $\Delta F(\chi)$, although the most part of $\Delta F(\chi)$ should come from the topological repulsive potential among LKs. It is remarkable that, although the magnitudes of $\Delta F(\chi)$ and $\Delta F_{\mathrm{SLM}}(\chi)$ are quite different, the difference between the isotropic and uniaxial condensation of $\Delta F(\chi)$ is roughly reproduced by $\Delta F_{\mathrm{SLM}}(\chi)$ (Fig. 7). This suggests that the difference between the isotropic and uniaxial condensation comes from a SL-model-like deformation of the chains.

To see this, we next consider conformational change of chains due to the macroscopic deformation of the system. It is represented by 'average extension ratio of the effective bond α_ξ, $\xi = x, y, z$' defined by

$$\alpha_\xi^2 = \langle l_{i,\xi}^2/a^2 L_i\rangle \text{ or } 12\langle[R_g^2]_{a,\xi}/\bar{b}^2 L_a\rangle, \qquad \xi = x, y, z, \tag{16}$$

where $\bar{b}$, the effective bond length of BF model, $[R_g^2]_{a,\xi}$, the ξ-component of R_g^2 of ring chain a (in the catena network) and $\langle\ \rangle$ represents the average over the time and chain a or strand i (in SL model). For SL model, they are given in the approximation, Eq. (14), by

$$\alpha_\xi^2(\chi) = \chi^{1/3} \qquad \text{for } \xi = x, y, z \text{ (isotropic)}. \tag{17}$$

$$\alpha_\xi^2(\chi) = \left\{\begin{matrix} \chi^{-1} & \text{for } \xi = x \\ \chi & \text{for } \xi = y, z \end{matrix}\right\} \text{(uniaxial)}. \tag{17'}$$

With use of $\alpha^2(\chi) = \alpha_x^2(\chi) + \alpha_y^2(\chi) + \alpha_z^2(\chi)$, Eq. (15) is rewritten by

$$\beta\Delta F_{\mathrm{SLM}}(\chi) = \frac{3\nu_s}{2}[\alpha^2(\chi)/3 - 1 - \ln\chi], \tag{18}$$

both for the isotropic and uniaxial deformation. In Fig. 9, $\alpha_\xi^2(\chi)$ determined by the simulation (shown by symbols) are compared with Eqs. (17) and (17′) (shown by lines); for the isotropic deformation, $\alpha^2(\chi)/3$ is plotted. As seen from Fig. 9, Eqs. (17) and (17′) give reasonable agreement with the simulation results, although they are overestimated considerably. Overestimation may be due to approximat Eq. (14), which restricts free rearrangement of the slip-links in the space and along the chains to minimize $\Delta F_{\mathrm{SLM}}(\chi)$ under a given macroscopic condition; therefore, $\Delta F_{\mathrm{SLM}}(\chi)$ given by Eqs. (17) and (17′) must also be overestimated. This may be the reason why the difference of $\Delta F_{\mathrm{SLM}}(\chi)$ between the uniaxial and isotropic deformation is a little larger than that of $\Delta F(\chi)$ as shown in Fig. 7.

Since the conformational changes represented by $\alpha_\xi^2(\chi)$ occur really and they are well described by SL model, $\Delta F_{\mathrm{SLM}}(\chi)$ must be a part of $\Delta F(\chi)$. However, there are large differences between $\Delta F(\chi)$ and $\Delta F_{\mathrm{SLM}}(\chi)$, as shown in Fig. 7, so that the main part of $\Delta F(\chi)$ should come from the topological repulsive potential among LKs. Since the topological repulsive potentials act along chains, they are insensitive to geometrical differences of macroscopic deformations (say, uniaxial or isotropic), which are approximately represented by SL model. Although $\Delta F_{\mathrm{SLM}}(\chi)$ is a part of $\Delta F(\chi)$, it is only a small correction term. RM studied the surface melting phenomena of lamella using SL model [11,12] but their work is insufficient because $\Delta F_{\mathrm{SLM}}(\chi)$ is just a small part of $\Delta F(\chi)$. This problem will be studied using $\Delta F(\chi)$ in the next paper [6].

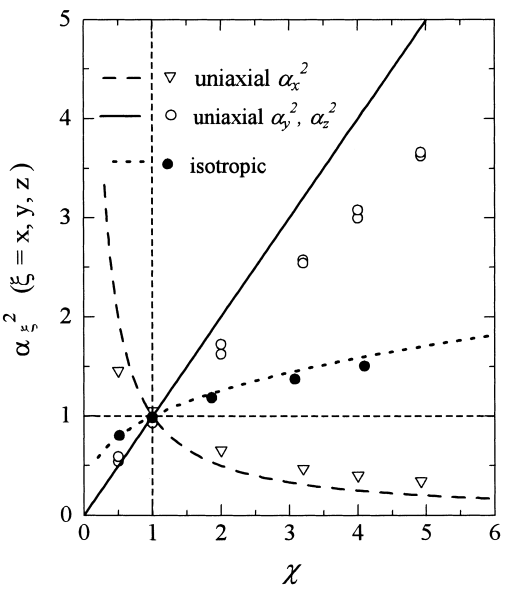

Fig. 9. Change of R_g^2 due to macroscopic deformation of the system, $a_\alpha^2(\chi) = \langle 12[R_g^2]_{a,\alpha}/L_a\rangle$, $\alpha = x, y, z$.

6. Determination and classification of Local-knots in the system

6.1. Average chain-length $\bar{L}_a(\chi)$

Another evidence for the repulsive potential among LKs is found in average chain-length $\bar{L}_a(\chi)$, $a = 1, 2, \ldots, N_p$. Due to the element-exchange reaction, L_a changes and the system becomes polydisperse. This is what really occurs in amorphous domains of semi-crystalline polymers. In the topological equilibrium state, $\bar{L}_a^0[= \bar{L}_a(1)]$ takes a value between 347 and 659 as shown in Table 5 (sample S_3 is used). At each condensation ratio χ, $\bar{L}_a(\chi)$ is plotted against $\bar{L}_a^0$ in Fig. 10. As seen from the figure, $\bar{L}_a(\chi)$ forms straight lines of slop $1/\chi$ (within 0.3% of error) passing the origin; this means that $\bar{L}_a(\chi)$ is inversely proportional to χ in all the chains. To explain this result, it is natural to assume that a strong repulsive force is acting among LKs; i.e. to make the total repulsion energy minimum, LKs should distribute with an equal intervals along the chains. This means that $\bar{L}_a(\chi)$ should be linearly proportional to number m_a of LKs trapped in each chain. To confirm this, we next compute m_a using the method presented in the previous work [4].

6.2. Number m_a of LKs trapped in each chain

Let $I(s_a, s_b)$ be a local Gauss integral in regard to stem $C(s_a, s_a + \nu)$ and $C(s_b, s_b + \nu)$, the former composed of $\nu + 1$ elements from s_a to $s_a + \nu$ of chain a and the latter, of $\nu + 1$ elements from s_b to $s_b + \nu$ of chain b

$$I(s_a, s_b) = \frac{1}{4\pi} \int_{s_a}^{s_a+\nu} \int_{s_b}^{s_b+\nu} \times \frac{(\dot{\mathbf{r}}_a(s) \times \dot{\mathbf{r}}_b(s')) \cdot (\mathbf{r}_a(s) - \mathbf{r}_b(s'))}{|\mathbf{r}_a(s) - \mathbf{r}_b(s')|^3} \mathrm{d}s\, \mathrm{d}s', \quad (19)$$

where $\mathbf{r}_a(s)$, $\mathbf{r}_b(s')$, $\dot{\mathbf{r}}_a(s)$ and $\dot{\mathbf{r}}_b(s')$ are coordinates and tangent vectors along chain a and b [21]. Length of the stems, ν, should be near the entanglement spacing, N_e. Considering $N_e = 89$ of BF model ($\phi = 0.5$) found in the previous work [19], $\nu = 100$ is assumed in this work (see Appendix A). When stem $C(s_a, s_a + \nu)$ and $C(s_b, s_b + \nu)$ form a LK as shown in Fig. 1, $I(s_a, s_b)$ takes near integer values, $\pm 1, \pm 2, \ldots$ To find LKs formed between chain a and b, local maximums of $|I(s_a, s_b)|$ are searched for, sweeping s_a and s_b along the chains. When local maximums exceed certain positive number I_0 ($I_0 = 0.3$ assumed in this work), they are recorded in a LK-candidate list. Since I_0 is much smaller than unity, the list contains many temporary fluctuations of $I(s_a, s_b)$, which are not true LKs. To remove temporary fluctuations from the list, time evolution of the local maximums is traced for a sufficiently long time by the Brownian motion with the local motions alone. Tracing is continued for 25 Mut (mega unit times), during which period the mean-square displacement of LKs along the chains reaches ca. 20,000 [element^2] or LKs move ca. 1.6 N_e elements as an average. If local maximums of $I(s_a, s_b)$ are temporary fluctuations, their $|I(s_a, s_b)|$ go rapidly below I_0 and they are removed from the LK-candidate list. After continuing this process for a sufficiently long time, only true LKs remain in the list. This operation is called 'a full-search-and-tracing (fs&t) of LKs'.

The time-evolution of the number of local maximums, $N_{1\,\max}(t)$, is shown in Fig. 11, where $N_{1\,\max}(t)$ is the average of samples S_1 and S_2. Following the method used in the previous work [4], $N_{1\,\max}(t)$ is decomposed into three exponentially decaying terms, $N_{1\,\max}^{(i)} \exp(-t/\tau_{1\,\max}^{(i)})$, $i = 1, 2, 3$, where $N_{1\,\max}^{(i)}$ and $\tau_{1\,\max}^{(i)}$ are strengths and life times of the modes. $N_{1\,\max}^{(i)}$ and $\tau_{1\,\max}^{(i)}$ determined by the least-mean-square-fitting method are given in Table 4. Following the arguments in the previous work [4], the shortest-living term M_1 is assigned to the temporary fluctuations of $I(s_a, s_b)$, the second term M_2, which have considerably long life time $\tau_{1\,\max}^{(2)} = 4.64$ Mut, to the temporary LKs and the longest living mode M_3 ($\tau_{1\,\max}^{(3)} = 51.5$ Mut), to the true LKs. The true LKs correspond to the LKs, which contribute to the

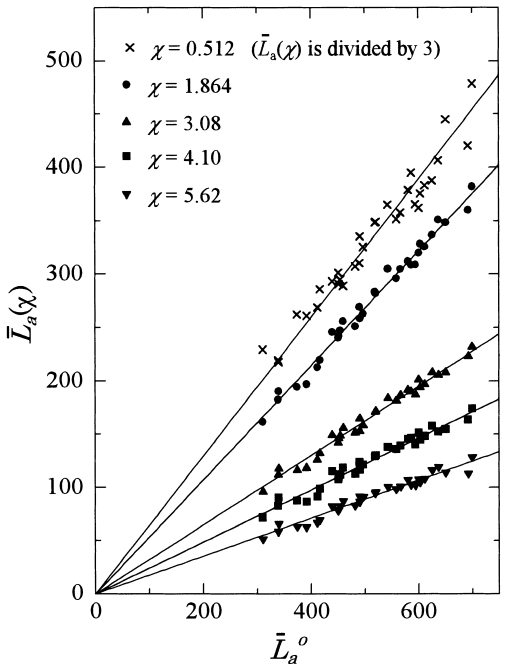

Fig. 10. Average length $\bar{L}_a(\chi)$ of chains $a(= 1, 2, \ldots)$ plotted against their topological equilibrium values $\bar{L}_a^0$. For $\chi = 0.512$, $\bar{L}_a(\chi)$ is divided by three in the figure. These data can be fitted by straight lines passing the origin and their slops are equal to $1/\chi$ within 0.3% of error.

Table 4
Decomposition of $N_{1\,\max}(t)$ into three exponentially decaying modes

Mode	$N_{1\,\max}^{(i)}$	$\tau_{1\,\max}^{(i)}$ (Mut)
M_1	460	0.37
M_2	206	4.64
M_3	296	51.5

Table 5
Average length $\bar{L}_a^0$ and effective number m_a of LKs trapped in each chain (sample 1)

Chain	$\bar{L}_a^0$	m_a
1	571	11
2	473	7
3	576	7
4	404	10
5	473	8
6	517	10
7	693	13
8	471	13
9	493	10
10	450	8
11	597	9
12	450	12
13	639	9
14	710	13
15	526	6
16	304	5
17	620	14
18	575	10
19	560	12
20	463	8
21	370	5
22	620	13
23	448	9
24	454	8
25	348	6
26	655	10
27	562	12
28	354	6
29	417	7
30	588	11
31	386	7
32	611	9
Total		298

repulsive potential considered here. The total number of the true LKs in the system is estimated to be $N_{\mathrm{LK}} = N_{\mathrm{l\,max}}^{(3)}/2 = 148$ or each chain contains 9.3 LKs as an average. The average chain length per LKs is estimated to be $\nu_{\mathrm{LK}} = 55$, which is close to 'the average chain length per entwining ring', $N_{\mathrm{e}}^* = 59$, found in the previous work [17]. Further discussions on the nature of LKs and the dissipation mechanism of $N_{\mathrm{l\,max}}(t)$ should be referred to Refs. [4,5].

Although true LKs have an essentially infinite lifetime, they are lost gradually in the tracing process. Dissipation of the true LKs occurs because $I(s_a, s_b)$ is not a true topological invariant; although their $I(s_a, s_b)$ stays most time near ± 1 (or near ± 2 in rare cases), it is not an exact constant of motion and, in the long tracing process, $|I(s_a, s_b)|$ fluctuates below I_0 and removed from the LK-candidate list. In the previous papers [5], it is argued that LKs behave like quantum mechanical particles and a kind of 'uncertainty principle' acts between their size ν and position s along the chains. Since ν is fixed, a very large fluctuation of s occurs in a long tracing process and our program loses sight of LKs (this phenomenon is called the 'probe fluctuation of LKs')

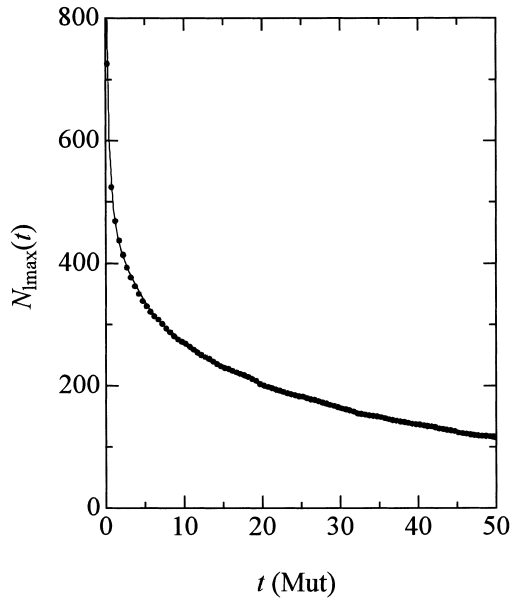

Fig. 11. Time evolution of number $N_{\mathrm{l\,max}}(t)$ of local maximums of $|I(s_a, s_b)|$. (average of sample 1 and 2).

[4–5]. Even if true LKs are lost in a process, they are found again by repeating fs&t in other periods. To cover the defect of the tracing program, fs&t is repeated five times with 5 Mut intervals. Since LKs are characterized by (1) their parent chains, (2) their signs and magnitudes of $I(s_a, s_b)$ and (3) their orders along the chains, LKs found in different fs&t are identified easily by these characteristic parameters. In counting LKs, relative position maps of LKs along the chains shown in Fig. 12 are used. In the maps, 32 chains existing in the system are designated by letters, '0'–'9' and 'A'–'X' ('I' and 'O' are omitted) and positions of LK, say that formed between chain A and B, are shown by letter 'B' in the LK-maps (lines of letters in the figure) of chain A and letter 'A', in those of chain B; in the maps, each letter occupies ca. 6.6 elements length along the chains; the five lines assigned for each chain show the average positions of LKs in the five fs&t periods. In Fig. 12, LK-maps of initial eight chains, 0–7, are shown as examples. The letters on the left end of lines (LK-maps) represent the standard LK for calculating the relative positions of LKs; in chain 0, for example, the standard LK is that formed between chain 0 and M, thus 'M' is printed on the left end of the line. In Fig. 12, local maximums of $|I(s_a, s_b)|$ survived longer than 3 Mut in each fs&t are shown. In this work, such LKs that appear at least in *three* of the five LK-maps of each chain are counted as true LKs; number m_a of true LKs thus found is given on the third column of Table 5. The total number of true LKs found by this method is equal to $N_{\mathrm{LK}} = 149$, which agrees well with $N_{\mathrm{LK}} = 148$ determined from the dissipation behavior of $N_{\mathrm{l\,max}}(t)$. Considering dissipation time $\tau_{\mathrm{l\,max}}^{(3)} = 51.6$ Mut of mode M_3, 5.6% of true LKs are lost in 3 Mut or the probability for them to be lost simultaneously in two of the five fs&t is essentially zero (0.2%); thus m_a

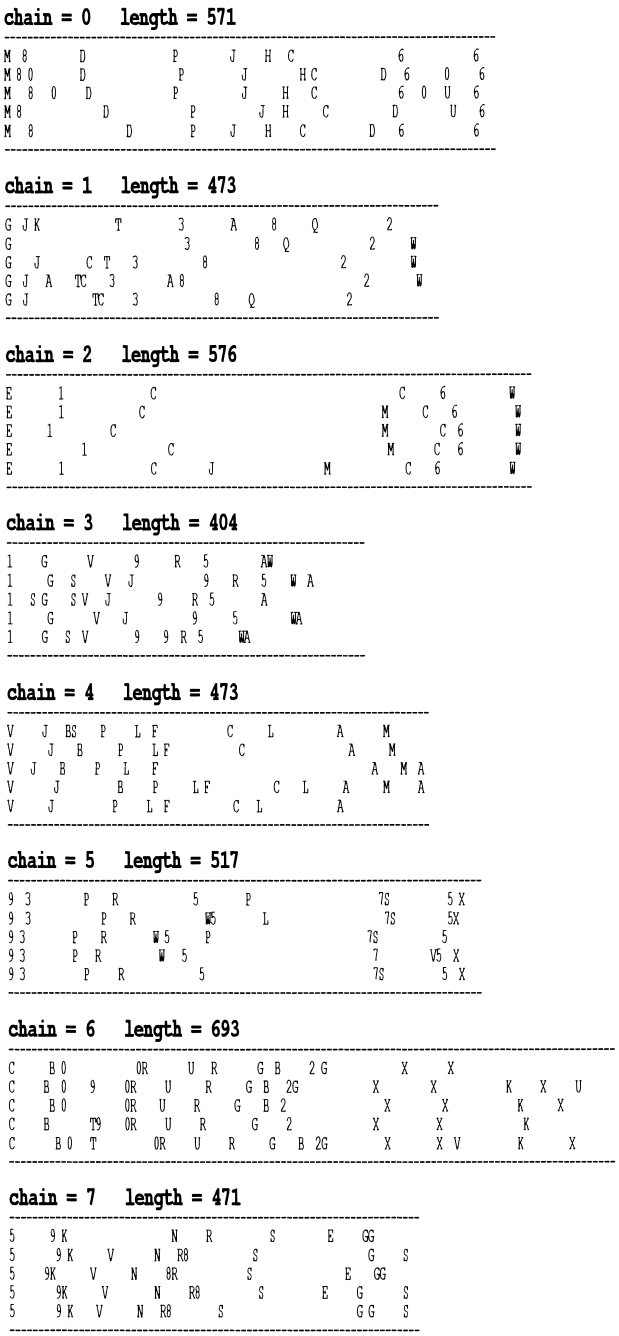

Fig. 12. LK-maps of initial eight chains, $a = 0, 1, \ldots, 7$.

given in Table 5 should contain almost all true LKs existing in the system. However, considering life time $\tau^{(2)}_{1\,\max} = 4.64$ Mut of the temporary LKs, ca. 4% of them must survive simultaneously in three fs&t; thus, Table 5 should contain ca. 3% of temporary LKs but this is within the error of the present calculations.

6.3. Relationship between m_a and $\bar{L}^0_a$

According to the above argument, $\bar{L}^0_a$ should be linearly proportional to m_a. To see this, $\bar{L}^0_a$ is plotted against m_a, $a = 0, 1, \ldots N_p$, in Fig. 13. As seen from the figure, $\bar{L}^0_a$ is

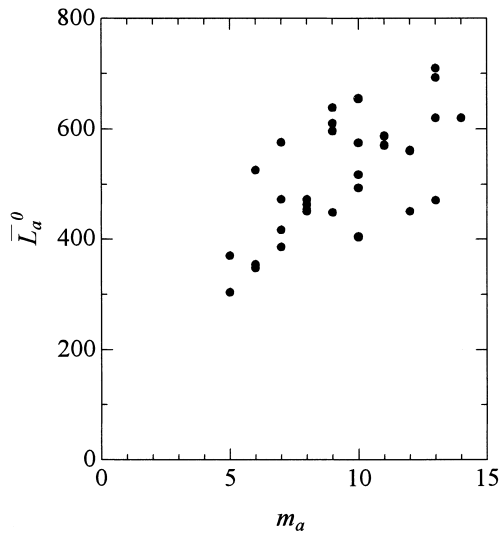

Fig. 13. Average chain-length $\bar{L}^0_a$ in the topological equilibrium state plotted against number m_a of LKs trapped in each chain a.

roughly proportional to m_a as expected, but the points are scattering widely from a linear line. Several reasons may be considered for this discrepancy. First, there are many kinds of LKs, such as shown in Fig. 14, which contribute differently to $\bar{L}^0_a$. In Fig. 14, LKs formed by n stems are designated as LK_n; LK_2 is further classified into $LK_{2,i}$, $i = 1, 2, \ldots$, according to the value of $|I(s_a, s_b)|$ (Fig. 14 A_1 and A_2). Complex $LK_n (n \geq 3)$ are found in the LK-maps. In Fig. 12, for example, three LK_3 ('7S' in chain 5, 'OR' in chain 6 and 'R8' or '8R' in chain 7) appear, in which two stems move synchronizing and overlapping with one another; although their synchronized motions are not so evident in the low-resolution map shown in Fig. 12, they are clearly observed in higher-resolution (in the position and time) maps, which are used to study the fine motions of LKs. Among the true LKs found, ca. 90% are of the simplest type, $LK_{2,1}$, and only a small number of complex LKs, such as $LK_{2,2}$, LK_3 and LK_4, are found; more complex $LK_{2,i}$ $(i \geq 3)$ or LK_n $(n \geq 5)$ are not found. For simple LK_2 ($LK_{2,i}$, $i = 1, 2, \ldots$), their orders along the chains are conserved;

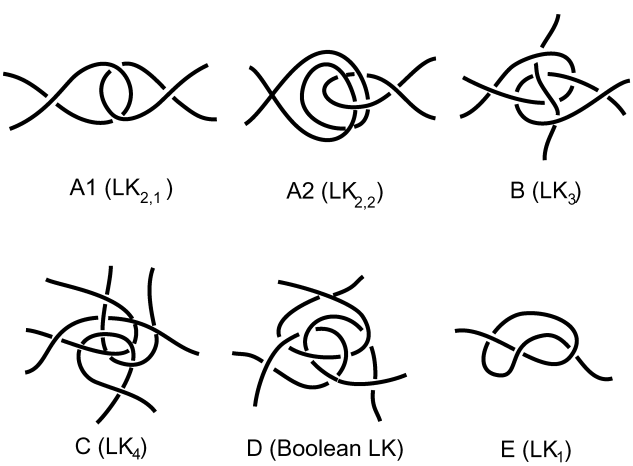

Fig. 14. Classification of local-knots.

when observed in the higher-resolution maps, their orders are sometimes disturbed but return rapidly to the original orders. In complex LK_n ($n \geq 3$), on the other hand, stems forming them overlap with one another and their orders along the chain are changing ceaselessly (when observed in the higher-resolution maps), so that they must form a complex LK as shown in Fig. 14B and C. However, the orders of all LKs along the chains are conserved, if the stems forming a complex LK are considered as a group. Volume of LKs occupying in the chains must changes with their complexities and, for simple LK_2s (A_1 and A_2 in Fig. 14), their volume must depend on their entwining number. In the present method, m_a gives such an effective number of LKs in which all the local maximums of $|I(s_a, s_b)|$ survived for the indicated period are counted as true LKs with equal weight; this corresponds to count LK of type LK_n with weight $n-1$ and the difference between the entwining number in LK_2 is neglected. Fig. 13 shows the relationship between $\bar{L}_a^0$ and m_a in this particular choice of the weight factors. However, the volume difference of LKs is not the main reason for the large scattering of the points in Fig. 13, because 90% of LKs are of the simplest type, $LK_{2,1}$, and mere change of their weights did not improve much the results.

The main reason for the discrepancy is that there are many voids in the LK-maps. In Fig. 12, two large voids appear between 'C' and 'M' in chain 2 and on the left side of '7S' in chain 5; smaller voids appear frequently, say, between 'D' and 'P' and between 'C' and 'D' in chain 0, between 'Q' and '2' in chain 1, between '1' and 'C' and between '6' and 'W' in chain 2, and so on. In these voids, there must be invisible LKs, which cannot be detected by the present tracing program using the Gauss integral. An example of such invisible LKs is shown in Fig. 14D, in which the Gauss integral gives almost zero for any pair of the three stems forming them, although they are evidently entangling with one another (14D is known as the Boolean link). It is well known in the topology of links that the Gauss integral cannot classify sufficiently complex links. To study the invisible LKs, higher topological invariants such as Alexander's polynomials must be used. Single-stem-knot LK_1s (or, simply, 'knots' in the legal terminology of topologists) shown in Fig. 14E are also invisible by the Gauss integral. LK_1s must appear frequently in the chains but they are qualitatively different from other LK_n ($n \geq 2$) from the following points: (1) they can pass through one another as well as through LK_ns ($n \geq 2$) and, (2) from this reason, the topological repulsion among LK_1s and between LK_1 and LK_n ($n \geq 2$) might be much weaker than that among LK_ns ($n \geq 2$). Study of these invisible LKs and single-stem-knot LK_1 is a matter of future works.

6.4. Validity of LK model

Although there remain these problems, the invisible LKs occupy only ca. 20% of the LK-maps or ca. 80% of LKs (in the volume fraction) are found in the present method; particularly, ca. 70% of LKs are the simplest LK_2 (A_1 in Fig. 14). We cannot observe the invisible LKs directly, but we can trace their motions indirectly by the motion of the voids, thus, can know the motion of all the LKs in the system. Therefore, we may conclude that the validity of LK model are probed sufficiently by the previous [4,5] and present simulations. Although there are differences among LKs in their volume occupying along the chains, in their strength of the topological repulsive potentials and in their mobility along the chain, this does not change the essential features of LK model. The wide scattering of the points from the linear relationship between $\bar{L}_a^0$ and m_a in Fig. 12 is explained by the existence of the invisible LKs; even if the all invisible LKs are included, an exact linear relationship between $\bar{L}_a^0$ and m_a may not be expected because there is the difference in the volume of LKs. The constant relationship of $\bar{L}_a(\chi)/\bar{L}_a^0$ shown in Fig. 11 and the origin of $\Delta\mu(\chi)$ and $\Delta F(\chi)$ are well explained by LKs, whether they are visible or not or whether they are large or small in volume and strength of the interaction potentials. In the previous works [4,5], $m_a (= \bar{\nu}_{LK}$ in the previous notation) is estimated from the ratio of diffusion coefficient D_{LK} of the collective motion (reptation motion) of LKs to diffusion coefficient D_{LK}^0 of single LK along a chain, assuming that all LKs have the same D_{LK}^0; actually, m_a determined in the previous work [4,5] gives an effective number of LKs, in which all LKs are converted into the simplest $LK_{2,1}$. Although there are many kinds of LKs, which contribute differently to $\bar{L}_a^0$, $\Delta\mu(\chi)$ and D_{LK} (even weight of LKs may be different in these quantities), there is no essential difference between the simplest $LK_{2,1}$ and other more complex LKs, except for single-stem-knot LK_1 which can pass through themselves as well as other LK_n, $n \geq 2$. LK model should be modified to include the differences among LKs, but it will give no large effect on the final results, because 70% (in the volume fraction) of LKs are the simplest $LK_{2,1}$. It is also reasonable to imagine that entangled polymer chains are composed mostly of $LK_{2,1}$ as shown in Fig. 1.

7. Concluding remarks

In this work, we have studied the motion of LKs in detail and found further evidences for the strong repulsive interaction among LKs. (1) Large deviations are found between $\Delta F(\chi)$ computed in this work and $\Delta F_{SLM}(\chi)$ predicted by the SL model in which the repulsive potentials among LKs are neglected; $\Delta F_{SLM}(\chi)$ should contribute partly to $\Delta F(\chi)$, but the most part of it must come form the repulsive potential among LKs. (2) It is found that average chain length $\bar{L}_a(\chi)$ is inversely proportional to condensation ratio χ and roughly proportional to number m_a of LKs trapped in each chain; these results also suggest the existence of strong repulsive forces acting among LKs along the chains. The most important feature of LK model is

that entanglement is composed of particles (LKs), which are countable and interacting with one another by repulsive forces along the chains. In this point, LK model is quite different from the usual tube model [14], which is considered as the standard model of entanglement. It will be shown in the next paper [6] that chemical potential change $\Delta\mu(\chi)$ due to condensation of entanglement play a central role in the crystallization problems of polymers. The particle nature of entanglement is the key to this problem; this is clearly seen in the step reaction (see figs. 10 and 11 of the next paper [6]) in which LKs trapped in an amorphous section of a chain are condensed as the crystallization proceeds. Such a model is possible only when entanglement is considered to be composed of particles (LKs).

Finally, it must be stressed that, although we have spend a lot of space discussing the nature of LK model, $\Delta\mu(\chi)$ given by Eq. (11) is determined independent of LK model, since the simulation model and Eq. (4) used in the calculation of $\Delta\mu(\chi)$ are independent of LK model. In this meaning, Eq. (11) is empirical equation. These equations are applied to crystalline polymers in the next paper [6].

Acknowledgements

We acknowledge support from a Grant-in-aid for Scientific Research from the Ministry of Education, Science and Culture, Japan (No. 07651100).

Appendix A

Following the method of the previous work [4], we actually used in the calculation a modified local Gauss integral

$$I^m(s_a, s_b) = \sum_{\xi=1}^{\nu} \sum_{\xi'=1}^{\nu} \sin(\xi\pi/\nu)\sin(\xi'\pi/\nu)\theta_{s_a+\xi, s_b+\xi'},$$

where $\theta_{i,j}$ is a Gauss integral in regard to bond $\mathbf{b}_i$ of chain a and bond $\mathbf{b}_j$ of chain b

$$\theta_{i,j} = \frac{1}{4\pi} \int_{i-1}^{i} \int_{j-1}^{j} \frac{(\dot{\mathbf{r}}_a(s) \times \dot{\mathbf{r}}_b(s'))\cdot(\mathbf{r}_a(s) - \mathbf{r}_b(s'))}{|\mathbf{r}_a(s) - \mathbf{r}_b(s')|^3} \mathrm{d}s\, \mathrm{d}s'.$$

$I(s_a, s_b)$ and $I^m(s_a, s_b)$ have almost the same nature but the latter moves more smoothly than the former so that the prove fluctuation of $I^m(s_a, s_b)$ is depressed a little, this makes tracing of $I^m(s_a, s_b)$ more easy. For $I^m(s_a, s_b)$, stem length ν should be considerably larger than N_e, so that $\nu = 100$ is used in the present work (compare it with $N_e = 89$). In the previous work [4], ν is changed widely but the results are the same, except that extremely small or large ν makes the dissipation rate of LKs increase and difficult to trace them for a long period. $\nu = 100$ chosen here is near the most suitable value for tracing. In the text, $I(s_a, s_b)$ is used for the sake of simplicity but, strictly, it should be reread by $I^m(s_a, s_b)$.

References

[1] Iwata K, Edwards SF. Macromolecules 1988;21:2901.
[2] Iwata K, Edwards SF. J Chem Phys 1989;90:4567.
[3] Iwata K. Macromolecules 1991;24:1107.
[4] Iwata K, Tanaka M. J Phys Chem 1992;96:4100.
[5] Iwata K. J Phys Chem 1992;96:4111.
[6] Iwata K. Polymer 2002; 43.
[7] Manderkern L. In: Dosiere M, editor. Crystallization of polymers. The Netherlands: Kluwer Academic Publishers; 1993. p. 25–37.
[8] Tanabe Y, Strobl GR, Fischer EW. Polymer 1986;27:1147.
[9] Mutter R, Stille W, Strobl G. J Polym Sci, Polym Phys 1993;31:99.
[10] Albrecht T, Strobl G. Macromolecules 1995;28:5827.
[11] Mansfield ML. Macromolecules 1982;20:1384.
[12] Riger J, Mansfield ML. Macromolecules 1989;22:3810.
[13] de Gennes PG. Scaling concepts in polymer physics. Ithaca: Cornell University Press; 1979.
[14] Doi M, Edwards SF, The theory of polymer dynamics, Oxford: Clarendon Press; 1986.
[15] Edwards SF. Proc R Soc London Ser A 1967;91:513.
[16] Edwards SF. J Phys A 1968;1:15.
[17] Doi M, Edwards SF. J Chem Soc, Faraday Trans 1978;74:2.
[18] Paul W, Binder K, Heermann DW, Kremer K. J Phys II 1991;1:37.
[19] Tanaka M, Iwata K, Kuzuu N. Comput Theor Polym Sci 2000;10:299.
[20] Tanaka M, Kuzuu S, Imai S, Iwata K. Comput Theor Polym Sci 2000; 10:309.
[21] Iwata K. J Phys Chem 1993;97:3451.